A METHOD OF DETERMINING ATTITUDE FROM MAGNETOMETER DATA ONLY*

G. A. Natanson, S. F. McLaughlin, R. C. Nicklas
Computer Sciences Corporation

ABSTRACT

The paper presents a new algorithm to determine the attitude using only magnetometer data under the following conditions: (1) internal torques are known and (2) external torques are negligible. Torque-free rotation of a spacecraft in thruster firing acquisition phase and its magnetic despin in the B-dot mode give typical examples of such situations. A simple analytical formula has been derived in the limiting case of a spacecraft rotating with constant angular velocity. The formula has been tested using low-frequency telemetry data for the Earth Radiation Budget Satellite (ERBS) under normal conditions. Observed small oscillations of body-fixed components of the angular velocity vector near their mean values result in relatively minor errors of approximately 5 degrees. More significant errors come from processing digital magnetometer data. Higher resolution of digitized magnetometer measurements would significantly improve the accuracy of this deterministic scheme. Tests of the general version of the developed algorithm for a free-rotating spacecraft and for the B-dot mode are in progress.

*This work was supported by the National Aeronautics and Space Administration (NASA)/Goddard Space Flight Center (GSFC), Greenbelt, Maryland, under Contract NAS 5-31500.

1. INTRODUCTION

The idea of developing an attitude determination system using only three-axis magnetometer measurements has been attracting attention for many years, despite its relatively low accuracy. The light weight and low cost of such a system are usually considered its main advantages. For a spacecraft in low-attitude Earth orbit, Kalman filtering has been proven to be an effective tool to derive the attitude from magnetometer measurements with a 2-degree (deg) accuracy (see References 1 and 2).

This paper is intended to develop an attitude determination algorithm using only magnetometer measurements under contingency conditions such as loss of attitude control of spacecraft. Due to high-speed rotation of a spacecraft, all other sensors, such as Sun sensors or star trackers, would become unreliable. Our research was inspired by studies of the attitude motion of the Earth Radiation Budget Satellite (ERBS) during the July 2, 1987, control anomaly. An analysis of the playback data (see Reference 3), revealed that the stimulation of the Sun sensor by bright Earth during one of the real-time passes led to an initially incorrect conclusion about the spacecraft orientation in the post G-Rate mode.

Although the attitude control system does not utilize gyro measurements under normal conditions, our analysis showed that these measurements can be effectively coupled with the magnetometer data to determine the attitude when angular rates are lower than the saturation limits on gyro output. Nevertheless, to give a worst case, we also assume a gyro failure either because of exceeding the telemetry limit or like that recently experienced by the Cosmic Background Explorer (COBE).

Therefore, the problem is to determine the attitude using only magnetometer data with no a priori knowledge of the spacecraft orientation. The latter requirement makes this research essentially different from the previous studies of attitude determination from magnetometer-only data via the Kalman filtering (see References 1 and 2). This is because the dynamical equations must first be linearized near their approximate solution. The solution was assumed known in References 1 and 2, which discussed a spacecraft under normal conditions, whereas this paper is focused on development of a deterministic algorithm for making the first guess in a situation when the attitude of the spacecraft deviates substantially from the expectations. After an approximate solution is found through a deterministic algorithm, it could be improved using the filtering technique (see References 1 and 2).

We have identified the two most typical attitude acquisition phases likely to be encountered under the contingency conditions:

(1) No thruster firing acquisition phase (angular rates <0.2 degree/second (deg/sec))

(2) Thruster firing acquisition phase (spinning rates within 10-50 deg/sec)

Due to relatively small angular rates in phase 1, the control system can significantly affect the spacecraft tumbling and, as a result, several situations should be studied. The following operational modes have been identified as the most representative choices:

(1a) Magnetic despin of a spacecraft (the B-dot mode) (see References 4 and 5)

(1b) Control system turned-off

(1c) A "blind" control system randomly rocking the spacecraft

(1d) Stabilization of the spacecraft by means of nutation damping

For Phase 2, the control system is expected to play a relatively minor role, and, consequently, spacecraft tumbling is expected to be predominantly governed by the torque-free Euler equations.

The paper presents a new deterministic algorithm, which works under the conditions that (1) internal torques are known and (2) external torques are negligible. Environmental torques are expected to be negligible either because of large angular momentum of the spacecraft or when compared with internal torques. Thruster firing acquisition phase and the B-dot mode give typical examples of such situations. Also, the algorithm can be used (at least in principle) to determine the attitude of a spacecraft governed by a "blind" control system (operational mode (1c)), when momentum wheel and scanwheel speeds and electromagnetic dipole moments are available from the telemetry data.

2. ANGULAR RATE UNCERTAINTY CIRCLE (ARUC)

Let $\vec{B}^A$ and $\vec{B}^R$ be the vectors of geomagnetic field measured in the body-fixed and reference frames, respectively:

$$\underset{\approx}{A}\,\vec{B}^R = \vec{B}^A \tag{2-1a}$$

The time derivatives $\dot{\vec{B}}^A$ and $\dot{\vec{B}}^R$ of two vectors are connected by the relation

$$\underset{\approx}{A}\,\dot{\vec{B}}^R = \dot{\vec{B}}^A + \vec{\omega}^A \times \vec{B}^A \tag{2-1b}$$

where $\vec{\omega}^A$ is the angular velocity vector referred to the body-fixed frame and the attitude matrix $\underset{\approx}{A}$ represents the orientation of one frame with respect to another. The vector $\dot{\vec{B}}^A$ can be computed from two sequential magnetometer measurements $\vec{B}_1^A$ and $\vec{B}_2^A$ by using the finite-difference approximation. The vector $\dot{\vec{B}}^R$, like the vector $\vec{B}^R$ itself, is found from the geomagnetic field model, assuming that the position of the spacecraft in space is known.

If the angular velocity vector $\vec{\omega}^A$ can be extracted from gyro measurements, Equations (2-1a) and (2-1b) can be directly used to determine the attitude via the TRIAD

algorithm (see Reference 6), which implements the so-called "algebraic method" of three-axis attitude determination (see Reference 7).

If only magnetometer measurements are used, the set of Equations (2-1a), (2-1b) is incomplete. In particular, the projection of the angular velocity vector $\vec{\omega}^A$ on geomagnetic field can be arbitrarily changed without violating Equation (2-1b). It is shown below that the projection of $\vec{\omega}^A$ on the plane perpendicular to the vector $\vec{B}^A$ is restricted by Equations (2-1a), (2-1b) to a circle, referred to below as the Angular Rate Uncertainty Circle (ARUC). To determine the attitude, it is necessary to know the position of the latter projection on the ARUC (i.e., the angle Φ in Figure 1, explained below). This requires the third sequential magnetometer measurement, which makes it possible to compute the second derivative of the vector $\vec{B}^A$ with respect to time. The algorithm that allows one to unambiguously determine both the attitude matrix $\underset{\approx}{A}$ and the angular velocity error $\vec{\omega}^A$ is outlined in Section 3.

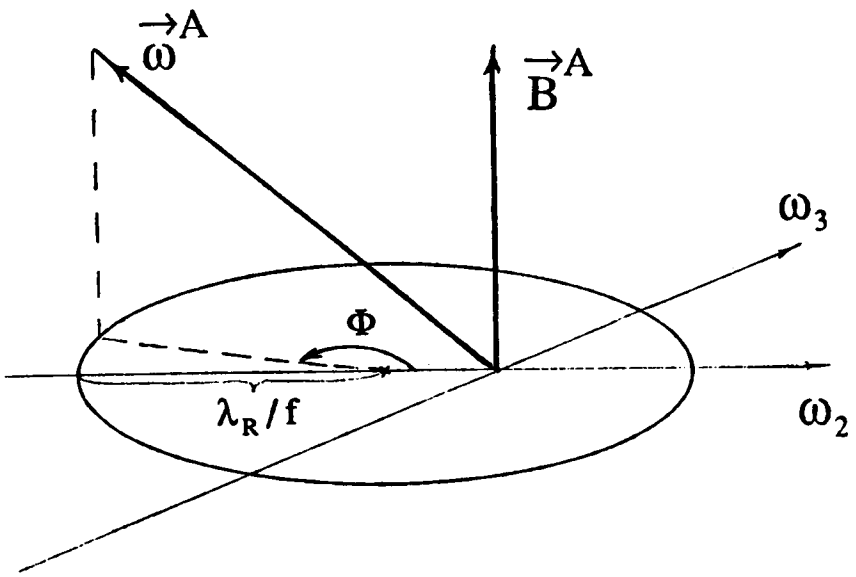

Figure 1. Angular Rate Uncertainty Circle (ARUC)

This section is focused on the information that can be extracted only from two sequential magnetometer measurements, giving rise to the particular ARUC. Calculating the square of magnitude of the vectors in the left- and right-hand sides of Equation (2-1) to exclude the attitude matrix, we come to the equation

$$|\dot{\vec{B}}^R|^2 - |\dot{\vec{B}}^A|^2 = |\vec{\omega}^A_\perp \times \vec{B}^A|^2 + 2\vec{\omega}^A_\perp \bullet (\dot{\vec{B}}^A \times \vec{B}^A) \qquad (2\text{-}2)$$

which contains only the projection $\vec{\omega}^A_\perp$ of the angular velocity vector $\vec{\omega}^A$ on the plane perpendicular to the geomagnetic field. (The vector $\vec{\omega}^A_\perp$ is referred to below as the transverse angular velocity.) Denoting the projections of $\vec{\omega}^A$ on the mutually perpendicular vectors,

$$\vec{D}_1 \equiv \vec{B}^A,\ \vec{D}_2 \equiv \vec{D}_1 \times \dot{\vec{B}}^A,\ \vec{D}_3 \equiv \vec{D}_1 \times \vec{D}_2 \tag{2-3}$$

by ω_1, ω_2, ω_3, one can easily see that the projections ω_2 and ω_3 lie on the circle:

$$(f\omega_2 + \lambda_A)^2 + f^2 \omega_3^2 = \lambda_R^2 \tag{2-4}$$

(See Figure 1). The parameters f, λ_A, and λ_R are defined as follows:

$$f \equiv |\vec{B}^R|/|\dot{\vec{B}}^R|,\ \lambda_A \equiv a \sin\psi_A,\ \lambda_R \equiv \sin\psi_R, \tag{2-5}$$

where

$$a \equiv |\dot{\vec{B}}^A|/|\dot{\vec{B}}^R| \tag{2-6}$$

and ψ_K (K = A, R) is the angle between the vectors $\vec{B}^K$ and $\dot{\vec{B}}^K$ (K = A, R). The center of the ARUC always lies in the left semiplane of the $\omega_2\,\omega_3$ plane. Depending on the value of the parameter a, the ARUC either lies completely in this semiplane (if $a > 1$) or crosses the ordinate at two points (if $a < 1$). For $a = 1$, the ARUC is tangent to the ordinate at the origin, and this is the only case when zero angular velocity is among the allowed solutions; otherwise, the spacecraft must rotate. The projection of angular velocity along the vector $\dot{\vec{B}}^A$ remains completely unrestricted unless the second derivatives of the geomagnetic field with respect to time are taken into account.

By analogy with the TRIAD algorithm (see Reference 6), we introduce three normalized reference vectors:

$$\hat{U}_1^R = \hat{B}^R,\ \hat{U}_2^R = \hat{U}_1^R \times \dot{\vec{B}}^R/(|\dot{\vec{B}}^R| \sin\psi_R),\ \hat{U}_3^R = \hat{U}_1^R \times \hat{U}_2^R \tag{2-7}$$

The crucial difference, however, comes from the fact that they can be transformed into their counterparts, $\hat{D}_1$, $\hat{D}_2$, $\hat{D}_3$ by the rotation $\underset{\approx}{A}$ only when the angular velocity vector is directed along the geomagnetic field.

It follows from Equation (2-7) that the unit vectors $\underset{\approx}{A}\,\hat{U}_2^R$ and $\underset{\approx}{A}\,\hat{U}_3^R$ are both orthogonal to the vector $\vec{B}^A$. As the same is true for the unit vectors $\hat{D}_2$ and $\hat{D}_3$ by definition, these two pairs of the mutually orthogonal vectors are related to each other as follows:

$$\underset{\approx}{A}\,\hat{U}_2^R = \cos\Phi\,\hat{D}_2 + \sin\Phi\,\hat{D}_3 \tag{2-8a}$$

$$\underset{\approx}{A}\,\hat{U}_3^R = -\sin\Phi\,\hat{D}_2 + \cos\Phi\,\hat{D}_3 \tag{2-8b}$$

where the angle Φ ranges between 0 and 2π. Introducing the 3-by-3 orthogonal matrix,

$$\underset{\approx}{T}_1(\Phi) \equiv \begin{bmatrix} 1 & 0 & 0 \\ 0 & \cos\Phi & -\sin\Phi \\ 0 & \sin\Phi & \cos\Phi \end{bmatrix} \tag{2-9}$$

Equations (2-8a) and (2-8b) can be represented in the matrix form

$$\underset{\approx}{A}\,\underset{\approx}{U} = \underset{\approx}{D}\,\underset{\approx}{T}_1(\Phi) \tag{2-10}$$

where $\underset{\approx}{D}$ and $\underset{\approx}{U}$ are 3-by-3 orthogonal matrixes having the vectors $\hat{D}_j$ and $\hat{U}_j$ (j = 1, 2, 3), respectively, as their columns,

$$\underset{\approx}{D} \equiv \left[\hat{D}_1 : \hat{D}_2 : \hat{D}_3\right], \quad \underset{\approx}{U} \equiv \left[\hat{U}_1^R : \hat{U}_2^R : \hat{U}_3^R\right] \tag{2-11}$$

Therefore,

$$\underset{\approx}{A} = \underset{\approx}{D}\,\underset{\approx}{T}_1(\Phi)\,\underset{\approx}{U}^{-1} \tag{2-12}$$

The angle Φ has a simple physical meaning; namely, it determines the position of the transverse angular velocity $\vec{\omega}_\perp^A$ on the ARUC. To prove this assertion, the vector $\vec{B}^A$ is written in terms of $\hat{D}_1$ and $\hat{D}_3$ using the relation

$$\hat{D}_3 = (\kappa_R \hat{D}_1 - \dot{\vec{B}}^A/|\dot{\vec{B}}^R|)/\lambda_A \tag{2-13}$$

which directly follows from the definition of the vector $\hat{D}_3$. This leads to the expression

$$\dot{\vec{B}}^A = |\dot{\vec{B}}^R| (\kappa_R \hat{D}_1 - \lambda_A \hat{D}_3) \tag{2-14}$$

Substituting Equation (2-14) in the right-hand side of Equation (2-1b) and representing $\vec{\omega}^A$ as $\omega_1 \hat{D}_1 + \omega_2 \hat{D}_2 + \omega_3 \hat{D}_3$ one finds

$$\underset{\approx}{A}\, \dot{\vec{B}}^R = |\dot{\vec{B}}^R| \left[\kappa_R \hat{D}_1 - \lambda_A \hat{D}_3 + f(\omega_3 \hat{D}_2 - \omega_2 \hat{D}_3)\right] \tag{2-15}$$

The vector $\dot{\vec{B}}^R$ in the left side of Equation (2-15) is expressed in terms of $\hat{U}_1^R$, $\hat{U}_3^R$ by analogy with Equation (2-14):

$$\dot{\vec{B}}^R = |\dot{\vec{B}}^R| \left[\kappa_R \hat{U}_1^R - \lambda_R \hat{U}_3^R\right] \tag{2-16}$$

Using Equation (2-8b) and comparing the coefficients of the vectors $\hat{D}_2$, $\hat{D}_3$ in both sides of the resulting equation, we get the relation:

$$f\omega_2 + \lambda_A = \lambda_R \cos\Phi, \quad f\omega_3 = \lambda_R \sin\Phi \tag{2-17}$$

that uniquely determines the transverse angular velocity $\vec{\omega}_\perp$ after the angle Φ is found. Coupled with Equation (2-12) for the attitude, this relation completes the information that can be extracted simply from Equations (2-1a), (2-1b), exploiting only two sequential magnetometer measurements.

3. USE OF THE SECOND DERIVATIVE OF GEOMAGNETIC FIELD WITH RESPECT TO TIME

In this section, we show how the position of the transverse angular velocity on the ARUC can be determined by using the second derivative of the geomagnetic field with respect to time in the case when body-fixed projections of the total torque acting on the spacecraft are known. To do it we differentiate Equation (2-1b) with respect to time and represent the resulting relation between second derivatives of the geomagnetic field measured in body-fixed and reference frames as

$$\underset{\approx}{A}\, \ddot{\vec{B}}^R = \ddot{\vec{B}}^A + \dot{\vec{\omega}}^A \times \vec{B}^A + 2\, \vec{\omega}_\perp^A \times \dot{\vec{B}}^A - \omega_\perp^2\, \vec{B}^A + \omega_1 \vec{C}_2 \tag{3-1}$$

where $\omega_\perp \equiv |\vec{\omega}^A_\perp|$ and

$$\vec{C}_2 \equiv 2\hat{D}_1 \times \dot{\vec{B}}^A + \hat{D}_1 \times (\vec{\omega}^A_\perp \times \vec{B}^A) \tag{3-2}$$

To calculate the second derivatives of the geomagnetic field, at least three measurements are needed: $\vec{B}^A_1$, $\vec{B}^A_2$, $\vec{B}^A_3$. To close the set of equations, it is also necessary to have an equation for $\dot{\vec{\omega}}^A$. As explained below, this equation can be easily included in the case of negligibly small external torques. Otherwise, it explicitly contains the unknown attitude matrix. The external torques can thus be taken into account only through an iterative procedure, which is vulnerable to measurement accuracy and may diverge.

For the particular case of constant angular velocity, $(\dot{\vec{\omega}}^A = \vec{0})$ projecting vector Equation (3-1) on the plane perpendicular to $\vec{C}_2$ makes it possible to exclude ω_1. It is convenient to use the same computation for the general case of nonzero $\dot{\vec{\omega}}^A$. The final equations are thus obtained by projecting vector Equation (3-1) on two mutually orthogonal unit vectors

$$\hat{C}_2 = [(\lambda_A + \lambda_R \cos \Phi)\, \hat{D}_2 + \lambda_R \sin \Phi \hat{D}_3]/c(\Phi) \tag{3-3}$$

and

$$\hat{C}_3 \equiv \hat{B}^A \times \hat{C}_2 = \left[(\lambda_A + \lambda_R \cos \Phi)\, \hat{D}_3 - \lambda_R \sin \Phi\, \hat{D}_2\right] /c(\Phi) \tag{3-4}$$

with

$$c(\Phi) = \sqrt{(\lambda_A + \lambda_R \cos \Phi)^2 + \lambda_R^2 \sin^2 \Phi} \tag{3-5}$$

(To derive Equation (3-3) from Equation (3-2) we used Equations (2-14) and (2-17) together with the definition of the vectors $\vec{D}_1$, $\vec{D}_2$, $\vec{D}_3$ (see Equation (2-3)). Note that there is no need to consider the equation obtained by projecting Equation (3-1) on the direction $\hat{B}^A$ of the magnetic field. In fact, Equation (2-2) shows that the projected equation can be represented as

$$\vec{B}^R \cdot \ddot{\vec{B}}^R + |\dot{\vec{B}}^R|^2 = \vec{B}^A \cdot \ddot{\vec{B}}^A + |\dot{\vec{B}}^A|^2 \tag{3-6}$$

Hence, it is equivalent to the first derivative of the equality $\vec{B}^R \cdot \dot{\vec{B}}^R = \vec{B}^A \cdot \dot{\vec{B}}^A$ with respect to time. Therefore, this projection simply describes the change in the parameters of the ARUC with time.

To compute the projections of the left-hand side, we first expressed the vectors $\vec{D}_2$, $\vec{D}_3$ in (3-3) and (3-4) in terms of $\underset{\approx}{A}\hat{U}_2^R$, $\underset{\approx}{A}\hat{U}_3^R$ from Equations (2-8a) and (2-8b). The final equations have the form

$$\delta_2(\Phi) - s_2(\Phi) = |\vec{B}|c(\Phi)\dot{\vec{\omega}}^A \cdot \hat{C}_3 + \omega_1(\Phi)|\dot{\vec{B}}^R|c^2(\Phi) \tag{3-7a}$$

$$\delta_3(\Phi) - s_3 = -|\vec{B}|c(\Phi)\dot{\vec{\omega}}^A \cdot \hat{C}_2 \tag{3-7b}$$

where

$$s_2(\Phi) \equiv -4\omega_3(\Phi)\lambda_A |\dot{\vec{B}}^R|\kappa_R \tag{3-8a}$$

$$s_3 \equiv -2\kappa_R|\dot{\vec{B}}^R|(1-a^2)/f \tag{3-8b}$$

and

$$\delta_2(\Phi) = \lambda_R\Delta_2^R - \lambda_A\Delta_2^A + (\lambda_A\Delta_2^R - \lambda_R\Delta_2^A)\cos\Phi - (\lambda_A\Delta_3^R + \lambda_R\Delta_3^A)\sin\Phi \tag{3-9a}$$

$$\delta_3(\Phi) = \lambda_R\Delta_3^R - \lambda_A\Delta_3^A + (\lambda_A\Delta_3^R - \lambda_R\Delta_3^A)\cos\Phi + (\lambda_A\Delta_2^R + \lambda_R\Delta_2^A)\sin\Phi \tag{3-9b}$$

with

$$\Delta_j^A \equiv \hat{D}_j \cdot \ddot{\vec{B}}^A, \qquad j = 2, 3 \tag{3-10a}$$

$$\Delta_j^R \equiv \hat{U}_j^R \cdot \ddot{\vec{B}}^R, \qquad j = 2, 3 \tag{3-10b}$$

The most important feature of Equations (3-7a), (3-7b) is that they do not contain the attitude matrix. The derived equations must be solved together with the dynamic equations of motion which make it possible to express $\vec{\omega}^A$ and $\dot{\vec{\omega}}^A$ in terms of torques. The full set of equations is closed provided that the torques are known.

3.1 CONSTANT ANGULAR VELOCITY

For constant angular velocity, the right-hand side of Equation (3-7b) vanishes and the resulting equation is transformed to a quadratic equation:

$$a_0 + 2a_1x + a_2x^2 = 0 \tag{3-11}$$

by the substitution $x = \tan(\Phi/2)$. The coefficients a_y ($y = 0,1,2$) in Equation (3-11) are defined as follows:

$$a_0 \equiv (\lambda_A + \lambda_R)(\Delta_3^R - \Delta_3^A) - s_3 \tag{3-12a}$$

$$a_1 \equiv \lambda_A\Delta_2^R + \lambda_R\Delta_2^A \tag{3-12b}$$

$$a_2 \equiv (\lambda_R - \lambda_A)(\Delta_3^R + \Delta_3^A) - s_3 \tag{3-12c}$$

After calculating two roots x_1 and x_2 of quadratic Equation (3-11) and substituting the appropriate values $\Phi_1 = 2 \arctan x_1$, $\Phi_2 = 2 \arctan x_2$, of the angle Φ in Equation (2-12), two possible solutions $\underset{\approx}{A}(\Phi_1)$ and $\underset{\approx}{A}(\Phi_2)$ for the attitude matrix are found. To select the correct solution it is necessary to calculate the angular velocity vector $\vec{\omega}^A(\Phi)$ for $\Phi = \Phi_k$, ($k = 1, 2$), using Equation (2-17) for $\omega_2(\Phi_k)$, $\omega_3(\Phi_k)$ and Equation (3-7a) for $\omega_1(\Phi_k)$:

$$\omega_1(\Phi_k) = [\delta_2(\Phi_k) - s_2(\Phi_k)]/[|\dot{\vec{B}}^R|c^2(\Phi_k)] \tag{3-13}$$

Taking into account that $\hat{B}^A = \underset{\approx}{A}(\Phi)\hat{B}^R$ for any point Φ on the ARUC (regardless of any error in data), the loss function is written as

$$L_{1,3}(\Phi_k) = \left[|\vec{B}_1^A - \underset{\approx}{A}^-(\Phi_k)\vec{B}_1^R| + |\vec{B}_3^A - \underset{\approx}{A}^+(\Phi_k)\vec{B}_3^R|\right]/(2\,dt) \tag{3-14}$$

where the matrices $\underset{\approx}{A}^-(\Phi_k)$ and $\underset{\approx}{A}^+(\Phi_k)$ are obtained by analytical propagation (see Equation (12-7b) in Reference 8) of the attitude backward ($t = -dt$) and forward ($t = dt$) in time t with constant angular velocity $\vec{\omega}^A(\Phi_k)$, starting from the matrix $\underset{\approx}{A}(\Phi_k)$ and assuming an equal time step dt between each sequential measurement. The correct root of Equation (3-11) is expected to give a smaller value for function (3-14), if all the time derivatives used in the algorithm are calculated accurately enough.

3.2 KNOWN INTERNAL TORQUES

Assuming that external torques are negligible, dynamic equations of motion are written as

$$\vec{N} = \underset{\approx}{I}\,\dot{\vec{\omega}}^{A} + \vec{\omega}^{A} \times \underset{\approx}{I}\,\vec{\omega}^{A} \tag{3-15}$$

where $\underset{\approx}{I}$ is the moment of inertia tensor and the internal torque $\vec{N}$ is a known function either of time or of the geomagnetic field. Two most important examples are torque-free rotation ($\vec{N} \equiv \vec{O}$) and the B-dot mode (see References 4 and 5). Expressing the components of the vector $\vec{\omega}^{A}$ as quadratic polynomials of $\omega_1(\Phi), \omega_2(\Phi), \omega_3(\Phi)$ from Equation (3-15) and substituting the resulting expressions in Equation (3-7a) gives the quadratic equation for ω_1 with coefficients dependent on Φ. Each of two roots $\omega'_1(\Phi)$ and $\omega''_1(\Phi)$ of this quadratic equation is then substituted in Equation (3-7b), giving rise to two transcendental equations. After all possible solutions Φ_k of both transcendental equations are found, together with the appropriate vectors $\vec{\omega}^{A}(\Phi_k)$ and $\dot{\vec{\omega}}^{A}(\Phi_k)$, they are tested using loss function (3-14), where the matrices $\underset{\approx}{A}^{-}(\Phi_k)$ and $\underset{\approx}{A}^{+}(\Phi_k)$ are obtained by propagating numerically both the attitude and the angular velocity vector backward and forward in time, starting from the matrix $\underset{\approx}{A}(\Phi_k)$ and assuming the vector $\dot{\vec{\omega}}^{A}(\Phi_k)$ to be constant. Again the solution sought is expected to give the smallest value for loss function (3-14).

4. TESTS OF THE ALGORITHM

Both the algorithm and its software implementation have been tested for the ERBS in the arbitrarily selected time interval from 890115.000025 to 890115.005937. Geocentric inertial coordinates (GCI) were used as the reference frame. The observed attitude matrices $\underset{\approx}{A}$ were constructed with the same time step of 8 sec as that used in the processed engineering data (low-frequency format) containing both the magnetometer measurements $\vec{B}^{A}$ and the model geomagnetic field $\vec{B}^{R}$ in the GCI. The angular velocity $\vec{\omega}^{A}$ was calculated by numerically differentiating the matrix function $\underset{\approx}{A}(t)$ with respect to time t.

As the first step, oscillations of the body-fixed components of the angular velocity vector near its average value of [-0.018, 0.049, -0.034] deg/sec were neglected and propagation of the attitude matrix was performed analytically, assuming constant angular velocity. The body-fixed projections of the geomagnetic field were computed by means of Equation (2-1a), using the analytically calculated attitude matrix and the model geomagnetic field read with a time step of either 8 or 16 sec.

In Figure 2, we present two solutions of Equation (3-11) as functions of time t. The small plateau in the upper curve represents the region where discriminant becomes negative due to numerical errors in the vectors $\vec{B}^{A}$ and $\vec{B}^{R}$ evaluated using the finite-difference approximation. At these points, the program simply sets the discriminant equal to zero (see Figure 3) and picks up both solutions from the previous time step. The small spike in the

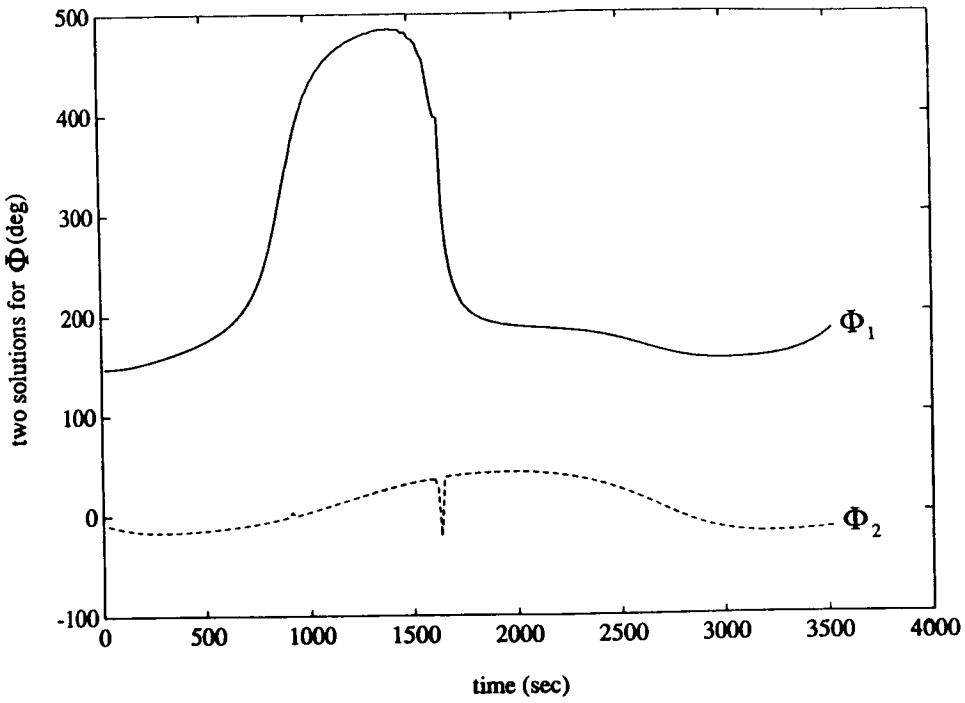

Figure 2. Test for Constant Angular Velocity (Step = 16 sec)

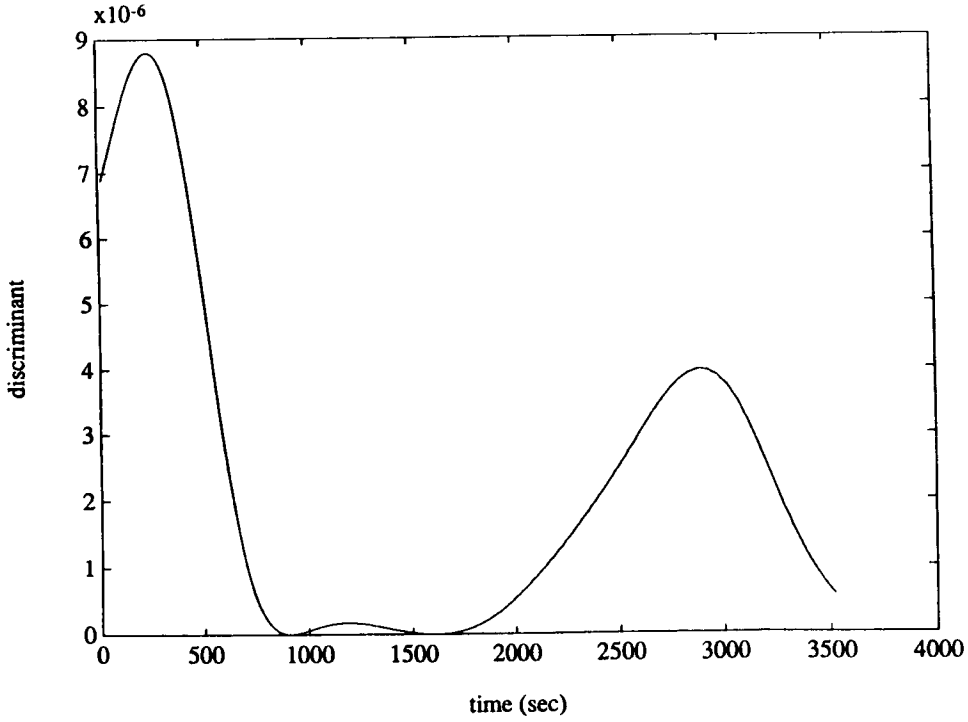

Figure 3. Test for Constant Angular Velocity (Step = 16 sec)

curve $\Phi_2(t)$ in Figure 2 at approximately 900 sec takes place where the discriminant illustrated in Figure 3 first touches the abscissa. The values of loss function (3-14) for each solution are presented in Figure 4. Due to errors in the time derivatives, two curves cross each other, and as a result, loss function (3-14) can be used to select the correct solution only in the region where the discriminant of quadratic Equation (3-11) is large.

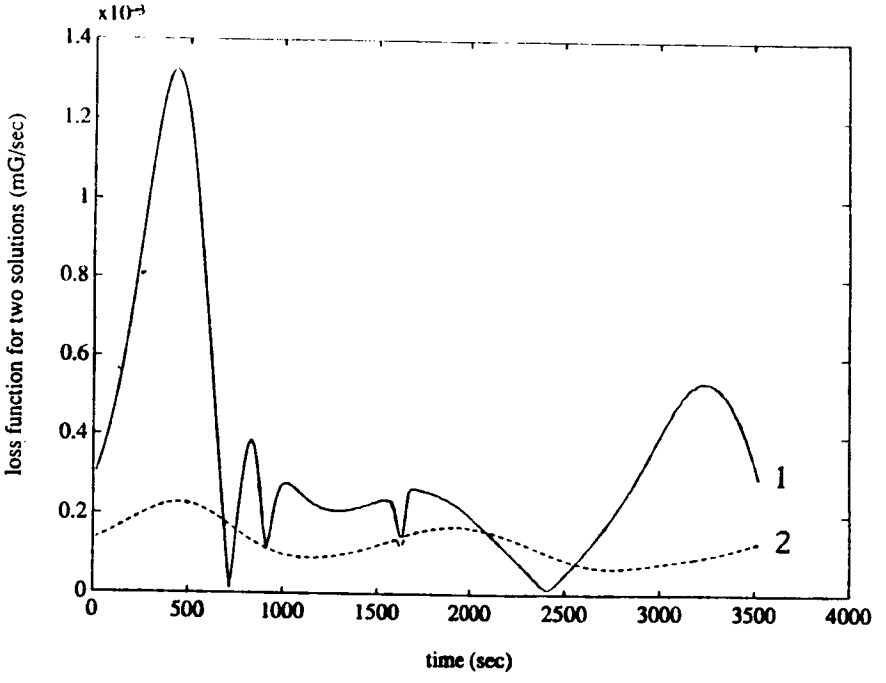

Figure 4. Test With Constant Angular Velocity (Step = 16 sec)

The attitude matrix $\underset{\approx}{A}$ is described here by a (212′) sequence of Euler rotations, using analytical formulae similar to Equations (12-21a) through (12-21c) in Reference 8. The values of the Euler angles determined by means of the developed algorithm are represented in Figure 5 by solid lines. The dot-dashed lines in Figure 5 represent the expected values in the limit of an infinitely small time step (the Euler angles were obtained from the analytically calculated attitude matrix). The agreement is reasonably good, except for the spikes in the region of significantly negative discriminant. It is worth mentioning that the small spikes observed in two upper curves in Figure 5 at approximately 900 sec completely disappeared when the smaller step of 8 sec was used to calculate the time derivatives of the geomagnetic field. This observation is in agreement with our statement that the observed errors are caused by a relatively large time step used for evaluating these derivatives.

The solid lines in Figure 6 present the components of the angular velocity vector obtained by numerically differentiating the attitude matrix derived from the low-frequency telemetry data. The dot-dashed straight lines show the average values that were used for propagation of the attitude matrix in the tests discussed above. Despite the fact that high-frequency oscillations are relatively small, they essentially affect the attitude, as clearly seen from Figure 7, where the solid lines are the observed values of the Euler angles, and the dot-dashed curves are from Figure 5. The physical significance of the

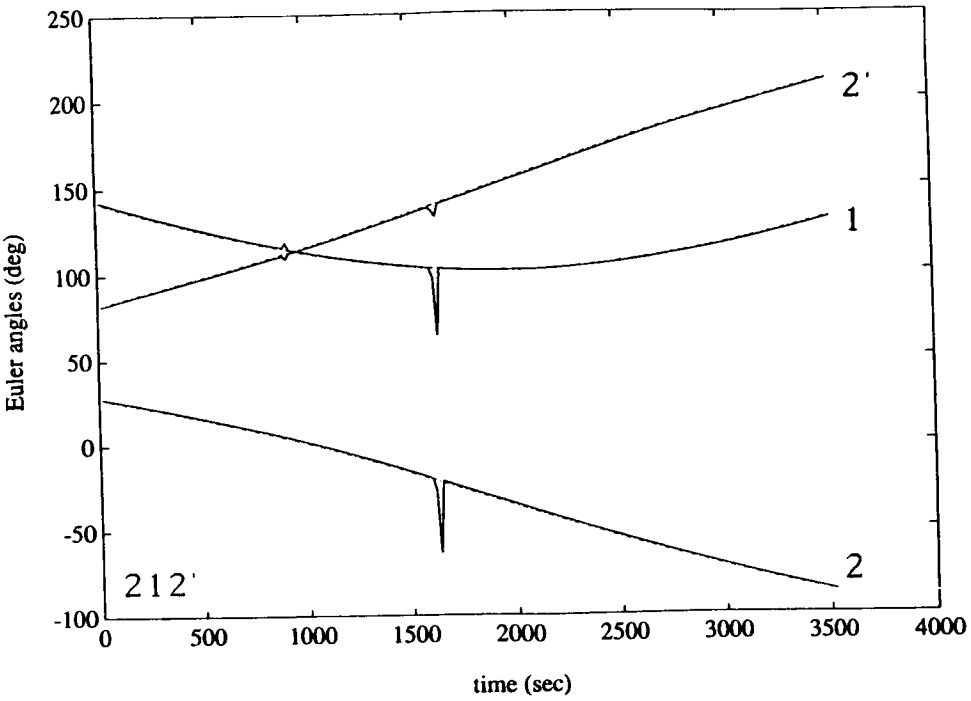

— · — · — Propagated attitude

——— Attitude determined from Equation (3-11)

Figure 5. Test for Constant Angular Velocity (Step = 16 sec)

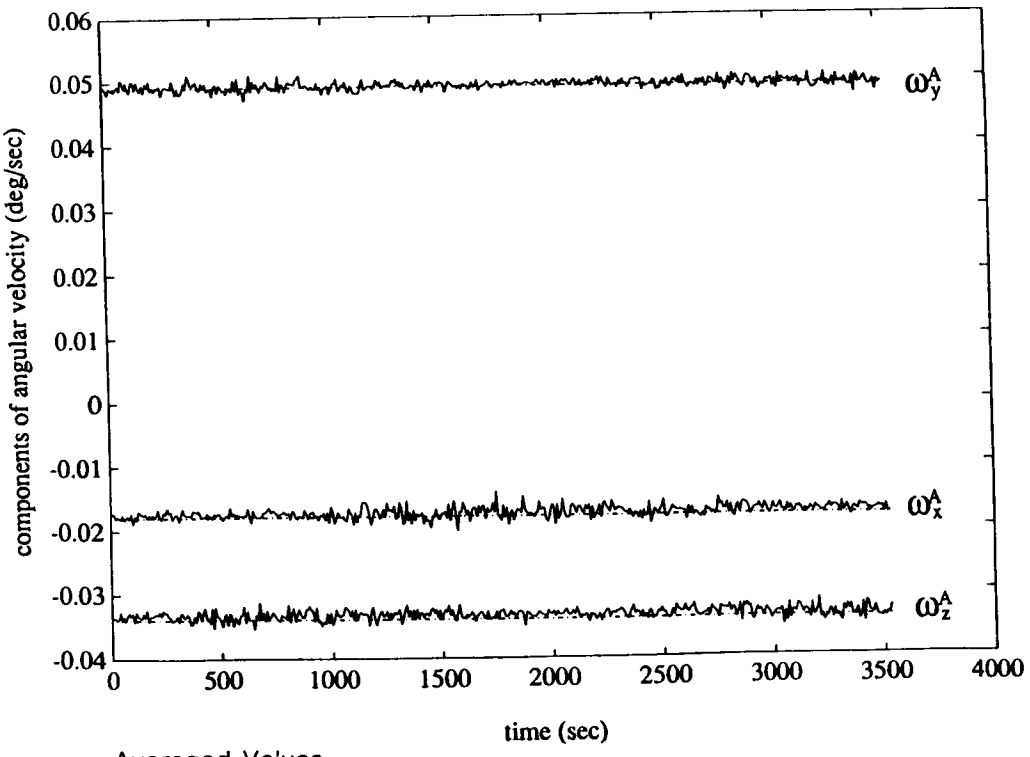

— · — · — Averaged Values

——— Extracted from the telemetry data

Figure 6. Measured/Averaged Angular Velocity

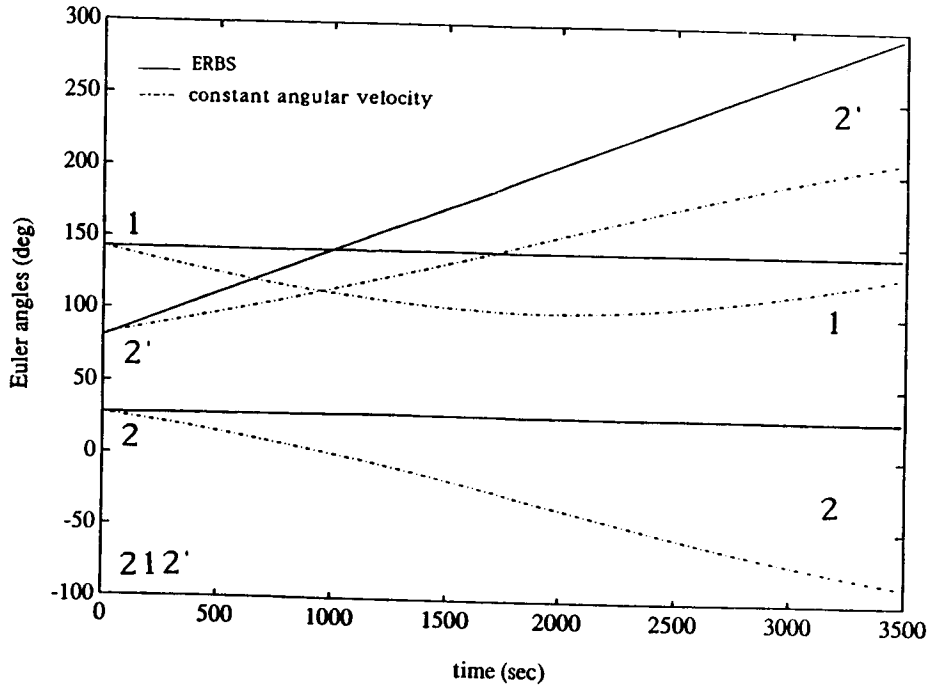

Obtained by propagating with the constant angular velocity

Extracted from the telemetry data

Figure 7. Effect of Averaging Angular Velocity

oscillations can be understood by analyzing behavior of the Euler angles 1 and 2, which determine the direction of the pitch body-fixed axis in the GCI (cf. Equation (12-20) in Reference 8). The oscillations simply force this direction to remain unchanged. It is remarkable that no oscillations are seen in the solid curves in Figure 7, despite the fact that the oscillations in angular velocity significantly affect the attitude.

In Figure 8, the magnetometer measurements taken from the low-frequency telemetry data are plotted versus the calculated body-fixed components of the geomagnetic field. The latter were obtained by rotating the geomagnetic field from the GCI frame to the body-fixed axes by means of the observed attitude matrix derived from telemetry data. The agreement looks reasonably good, except for the stepwise behavior of the measured data due to their analog-to-digital conversion with the increment of ~6.44 milligauss (mG). The coarse digitization of the magnetometer measurements creates an obstacle in calculating the second derivative $\ddot{B}^A$ of the geomagnetic field. This is illustrated by Figure 9, where the zigzag lines were obtained by processing the magnetometer measurements and the dash-dotted lines represent the second derivative of the calculated geomagnetic field with the same finite-difference scheme and the same time step of 240 sec used in both cases. The digitization results in relatively large errors of $\pm$20-deg in attitude determination. In Figure 10, we plot the determined Euler angles (solid lines) versus their observed values (dot-dashed lines) selected at a time step of 240 sec. In Figure 11, for comparison, we give a similar plot for the Euler angles which were determined by utilizing the attitude information in the telemetry data to model a field measurement in the body-fixed frame and then using this in the algorithm to show the upper limit on accuracy. In addition to the curves exploiting the time step of 240 sec (solid lines) to calculate the

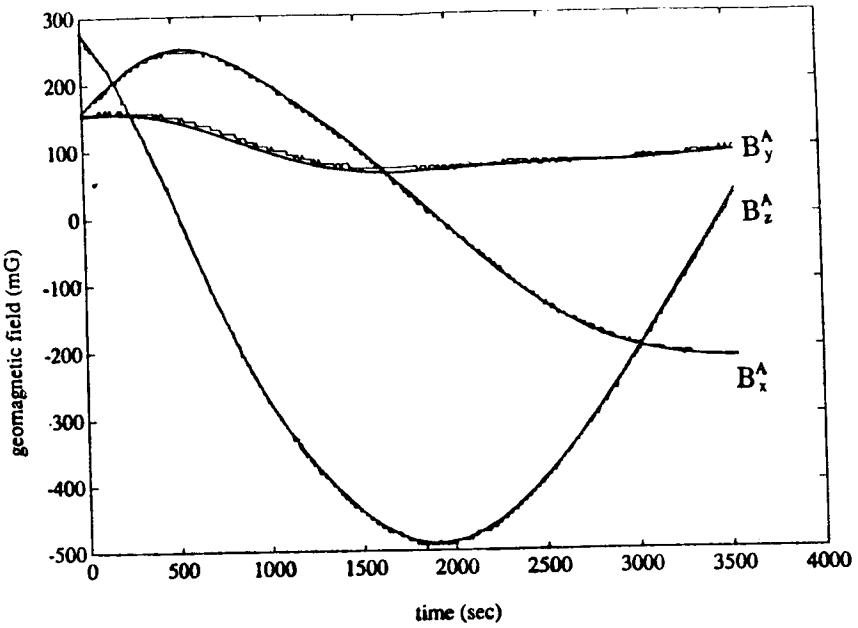

Stepwise lines show the magnetometer data; smooth curves were calculated by using Equation (2-1a).

Figure 8. Measured Versus Calculated Geomagnetic Field

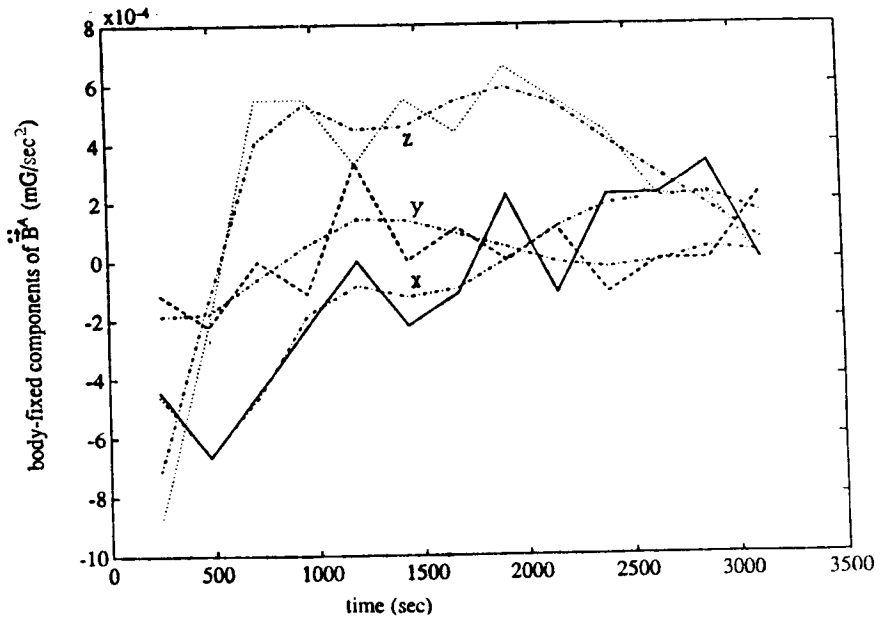

Zigzag lines obtained by processing the magnetometer data; smooth curves represent the second derivative of the calculated geomagnetic field with respect to time.

Figure 9. Second Derivatives of Measured Versus Calculated Geomagnetic Field With Respect to Time (Step = 240 sec)

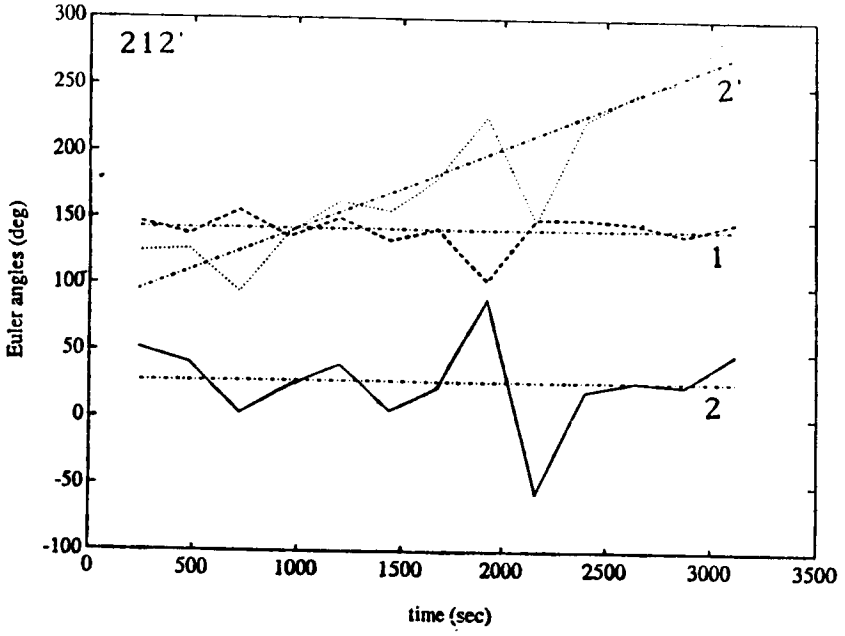

Zigzag lines show the Euler angles determined from the magnetometer data; dot-dashed lines show the Euler angles determined using the calculated body-fixed components at the geomagnetic field.

Figure 10. Use of Measured Geomagnetic Field (Step = 240 sec)

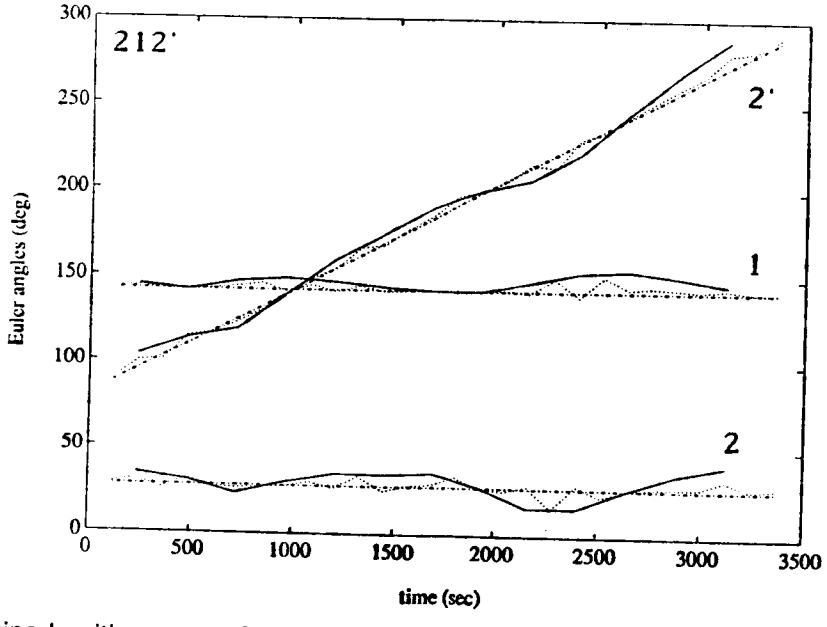

- - - - - Determined; with a step of 120 sec; —— · —— · —— observed

——— Determined; with a step of 240 sec

Figure 11. Use of Calculated Geomagnetic Field (Steps = 120, 240 sec)

necessary time derivatives, Figure 11 also reproduces the Euler angles determined using the time step of 120 sec (dotted lines). In the case of the measured geomagnetic field, use of the large step was necessary to smooth the data. However, it results in some systematic errors clearly seen in Figure 11. A further decrease in a time step used to compute the time derivatives of the calculated geomagnetic field results in accumulation of errors caused by oscillations of angular velocity, which are disregarded in the algorithm. Therefore, the time step of 120 sec turns out to be an optimum compromise, providing accuracy of ~5 deg for each angle.

The observed oscillations of the angular velocity vector significantly affected the ability of the algorithm to determine its body-fixed components. In Figure 12, the dashed and dotted lines show the values of these components determined using a time step of 120 sec, and the solid lines show the observed values selected at the same time step. The total angular rate of 0.062 deg/sec is reasonably well reproduced by the dominant y-component of the determined angular velocity vector, whereas the two remaining components are too small to contribute and are thus in obvious disagreement with the observations.

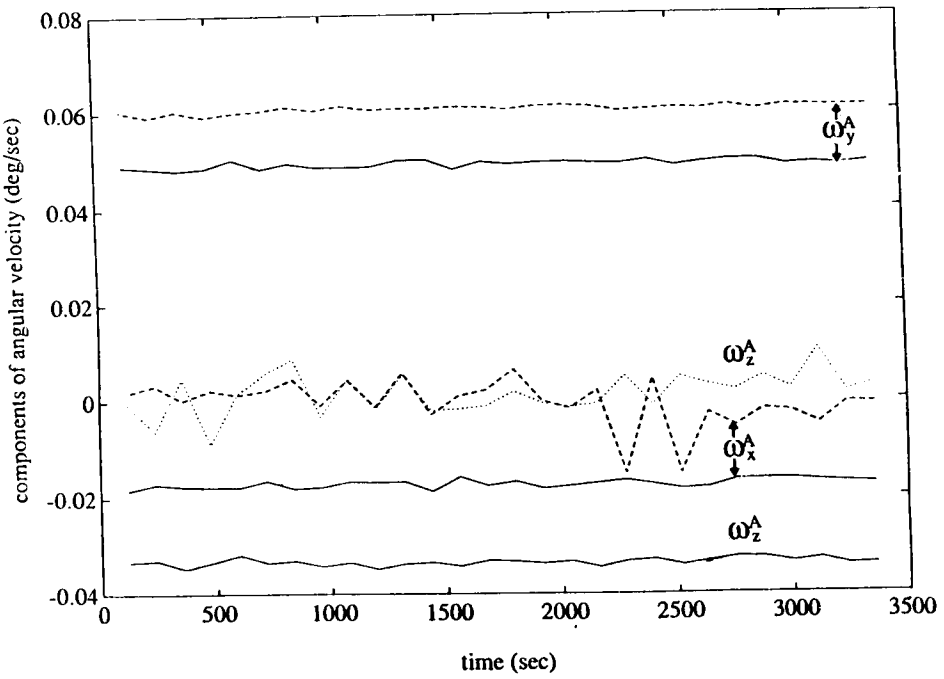

Zigzag lines show the values determined using the developed algorithm; solid lines show the observed values.

Figure 12. Use of Calculated Geomagnetic Field (Step = 120 sec)

5. CONCLUSIONS AND FURTHER DEVELOPMENTS

The reported preliminary analysis demonstrates that the deterministic approach to coarse attitude determination, using only magnetometer data, is feasible. A successful

implementation could benefit significantly from more accurate representation of magnetometer measurements in telemetry records than is provided for the ERBS.

Our study of the applicability of the algorithm to attitude determination under normal conditions is mostly methodological and illustrative. As mentioned in the introduction, the main objective is to develop an attitude determination system for application under contingency conditions when only magnetometer data are available. In particular, the analytical formula derived here for the limiting case of constant angular velocity could be applied to a spacecraft rotating around its major principal axis after it was stabilized using nutation damping. At this time, we are studying applicability of the developed algorithm to a spacecraft in the B-dot mode and to a spacecraft freely rotating with high angular speeds caused by thruster firing. The errors from neglecting environmental effects in both cases are now being investigated.

ACKNOWLEDGMENTS

The authors thank M. Phenneger for his guidance and extremely valuable critical remarks on the manuscript. One of the authors (G. A. Natanson) is also indebted to D. Chu for interesting, encouraging discussions, to F. L. Markley for his comments on the literature on magnetic despin of a spacecraft, and to B. Rashkin for his helpful suggestions on the presentation of the results.

REFERENCES

1. G. A. Heyler, "Attitude Determination by Enhanced Kalman Filtering Using Euler Parameter Dynamics and Rotational Update Equations," AIAA Paper No. A81-45832, AAS/AIAA Astrodynamics Specialist Conference, Lake Tahoe, Nevada, Aug. 3-5, 1981

2. F. Martel, P. K. Pal, and M. L. Psiaki, "Three-Axis Attitude Determination via Kalman Filtering of Magnetometer Data," Paper No. 17 for the Flight Mechanics/ Estimation Theory Symposium, NASA/Goddard Space Flight Center, Greenbelt, Maryland, May 10 and 11, 1988

3. J. Kronenwetter and M. Phenneger, *Attitude Analysis of the Earth Radiation Budget Satellite (ERBS) Control Anomaly*, CSC/TM-88/6154

4. A. C. Stickler and K. T. Alfriend, *Elementary Magnetic Attitude Control System*, Journal of Spacecraft, Volume 13, pp. 282-287, 1976

5. F. L. Markley "Attitude Control Algorithms for the Solar Maximum Mission," AIAA Paper No. 78-1247 for the 1978 AIAA Guidance and Control Conference, Palo Alto, CA 1978

6. M. D. Shuster and S. D. Oh, *Three-Axis Attitude Determination from Vector Observations*, J. Guidance and Control, 4, pp. 70-77, 1981

7. G. M. Lerner, "Three-Axis Attitude Determination," in *Spacecraft Attitude Determination and Control*, J. R. Wertz, ed. Dordrecht, Holland: D. Reidel Publishing Co., 1978, pp. 420-428

8. G. M. Lerner, "Parameterization of the Attitude," in *Spacecraft Attitude Determination and Control*, J. R. Wertz, ed. Dordrecht, Holland: D. Reidel Publishing Co., 1978, pp. 412-420